Distributed model-based sensor fault diagnosis of marine fuel engines

Kougiatsos, N.; Negenborn, R.R.; Reppa, V.

DOI
10.1016/j.ifacol.2022.07.153

Publication date
2022

Document Version
Final published version

Published in
IFAC-PapersOnLine

Available online at www.sciencedirect.com

ScienceDirect

IFAC PapersOnline CONFERENCE PAPER ARCHIVE

IFAC PapersOnLine 55-6 (2022) 347–353

Distributed model-based sensor fault diagnosis of marine fuel engines ⋆

Nikos Kougiatsos * **Rudy R. Negenborn** * **Vasso Reppa** *

* *Department of Maritime and Transport Technology, Faculty of Mechanical, Maritime and Materials Engineering, Delft University of Technology, 2628CD, the Netherlands,*
(e-mail: {n.kougiatsos, r.r.negenborn, v.reppa} @ tudelft.nl).

Abstract: This paper proposes a distributed model-based methodology for the detection and isolation of sensor faults in marine fuel engines. The proposed method considers a Mean Value First Principle model and a wide selection of heterogeneous sensors for monitoring the engine components. The detection of faults is realised based on residuals generated using nonlinear Differential Algebraic estimators combined with adaptive thresholds. The isolation of faults is, then, realised in two levels; local sensor fault detection and isolation agents are designed to monitor specific sensor sets and aim to detect faults in these sets; and a global decision logic is designed to isolate multiple sensor faults that may be propagated between the local monitoring agents. Finally, simulation results are used to illustrate the application of this method and its efficiency.

Keywords: Distributed Fault Diagnosis, sensor faults, Differential–algebraic equations (DAE's), nonlinear systems, Marine system modelling, interconnected systems

1. INTRODUCTION

Nowadays, the maritime industry is responsible for the transport of 90% of global cargo and the lives of more than a million seafarers and passengers worldwide. Ensuring their safety should be one of the priorities in the maritime field. However, recent statistics from the European Maritime Safety Agency (2020) suggest that 22% of the total ship casualties in 2019 was caused by the loss of propulsion, a situation which leaves the vessel ungoverned in the uncertain sea environment. Thus, the monitoring of marine engines is safety-critical [Aslam et al. (2020)].

Most literature has focused only on diagnosing fuel engines' process faults while sensors were mostly believed to report reliable information. However, sensor faults also occur and should be taken into consideration [Wu et al. (2006)]. Securing sensors' health should be treated as important as that of the engine itself since the decisions made after diagnosing a fault may differ in the case of a sensor fault and in that of a process fault [MACSEA (2012)]. A wrong decision during voyage could affect the lives onboard the vessel, the transported cargo and possibly the environment. In addition, due to the larger size of engines, limited operator access as well as the highly uncertain sea environment, the consequences of a bad decision regarding faults can be greater in a marine system than a land-based system [Wang et al. (2017)]. On top of that, the occurrence of multiple sensor faults has become a significant problem to tackle, due to the large number of sensors distributed in marine systems such as marine fuel engines [Jones and Li (2000)]. Although more realistic, this problem has not yet received much attention in the relevant literature.

In the area of sensor fault diagnosis for marine fuel engines there has already been some research activity. Mesbahi in his work [Mesbahi (2001)] applies an Artificial Neural Network (ANN) technique to validate the coherence of sensor measurements, isolate faulty sensors and recover the lost information from healthy measurements for a 6-cylinder engine. However, only single faults are considered and a massive amount of data is needed for training purposes in order to include both healthy and faulty conditions. Hu et al. (2018) on the other hand, perform temperature sensor fault detection for a selective catalyst reduction (SCR) system built upon a Diesel Engine using a suitable temperature model and an Extended Kalman Filter (EKF). Nonetheless, the authors choose an arbitrary threshold to perform fault detection, which may lead to missed detection of sensor faults or false alarms if it is not well selected. Finally, in [Wohlthan et al. (2021)], a model-based sensor fault diagnosis method is proposed for engine test beds using a multi-stage geometric analysis of the extracted residuals. However, this method considers static models and single sensor fault occurence.

The objective of this work is to design a model-based technique to detect and isolate the occurrence of faults affecting multiple sensors of marine fuel engines. As the system is very complex and consists of highly interconnected subsystems, a distributed monitoring approach is proposed. In particular, local Sensor Fault Detection and Isolation (SFDI) agents are designed (see Section 4), where each agent uses information from a specific sensor set and captures the occurrence of faults in these sensor sets.

⋆ This publication is part of the project READINESS with project number TWM.BL.019.002 of the research programme "Topsector Water & Maritime: the Blue route" which is partly financed by the Dutch Research Council (NWO).

10.1016/j.ifacol.2022.07.153

The detection of faults is realised by comparing a set of residuals to the designed adaptive thresholds while the isolation of sensor faults relies on a combinatorial decision logic [Reppa et al. (2016)]. The computation of residuals and adaptive thresholds is based on a Mean Value First Principle (MVFP) model (see Section 3) which can more accurately describe the actual engine. This model incorporates both differential and algebraic equations (DAE) (see Section 2).

From the application point of view, the main contribution of this research work is the development of a distributed SFDI architecture that manages to isolate multiple sensor faults in marine fuel engines. The use of adaptive thresholds allows to reduce the conservativeness in decision making, excluding false alarms. Moreover, the MVFP model provides a greater generalization ability of the results for different engines, since it can be easily reconfigured in its parameters and can also be expanded to host more subsystems and sensors. Compared to the state-of-the-art in distributed model-based fault diagnosis literature where mostly systems described by ordinary differential equations (ODE) are considered [Reppa et al. (2016); Boem et al. (2017); Keliris et al. (2015)], this work focuses on systems described by nonlinear DAE. The design of algebraic residuals and adaptive thresholds is a challenging task that affects the detectability of sensor faults.

2. PROBLEM FORMULATION

Marine fuel engines are complex systems incorporating components characterised by heterogeneous dynamics and inherent interconnections. In Fig. 1 a representation of a marine fuel engine is shown, where the different parts are grouped in four distinct subsystems and a total of ten sensors are deployed for condition monitoring. This work

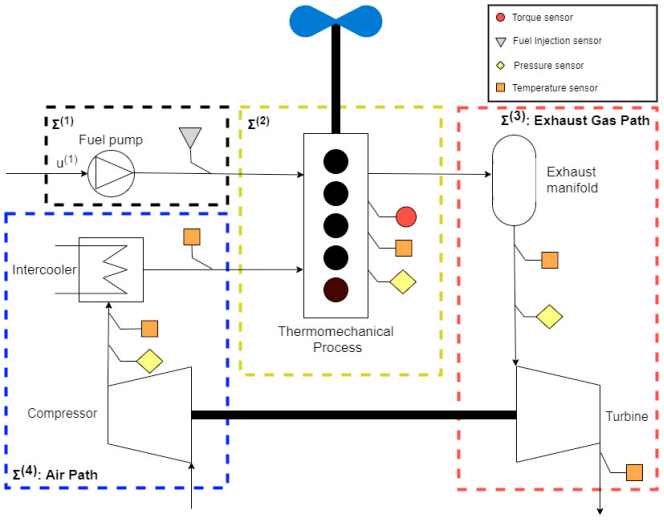

Fig. 1. Schematic representation of a typical marine fuel engine

aims to diagnose faults affecting more than one sensors in the marine fuel engine system.

Given the heterogeneous dynamics and interconnections of the subsystems in marine fuel engines, the proposed fault diagnosis method is developed considering a class of N nonlinear DAE-based interconnected systems $\Sigma^{(I)}, I = 1, \cdots, N$ described by [Vemuri et al. (2001)]:

$$\Sigma^{(I)}: \begin{cases} \dot{x}^{(I)}(t) = A^{(I)}x^{(I)}(t) + \gamma^{(I)}(x^{(I)}(t), z^{(I)}(t), u^{(I)}(t)) + \\ h^{(I)}(x^{(I)}(t), z^{(I)}(t), \chi^{(I)}(t), u^{(I)}(t)) + \eta_x^{(I)}(t), & \text{(1a)} \\ 0 = \xi^{(I)}(x^{(I)}(t), z^{(I)}(t), \chi^{(I)}(t), u^{(I)}(t)) + \eta_z^{(I)}(t) & \text{(1b)} \end{cases}$$

where $x^{(I)} \in \mathbb{R}^{n_I - r_I}$ is the state variable vector, $z^{(I)} \in \mathbb{R}^{r_I}$ is the algebraic variable vector, $\chi^{(I)} \in \mathbb{R}^{k_I}$ are the interconnection variables from the neighbouring subsystems, $u^{(I)} \in \mathbb{R}^{l_I}$ is the control input vector, $\gamma^{(I)} : \mathbb{R}^{n_I - r_I} \times \mathbb{R}^{l_I} \mapsto \mathbb{R}^{n_I - r_I}$ represents the known nonlinear system dynamics, $h^{(I)} : \mathbb{R}^{n_I - r_I} \times \mathbb{R}^{r_I} \times \mathbb{R}^{k_I} \times \mathbb{R}^{l_I} \mapsto \mathbb{R}^{n_I - r_I}$ represents the known interconnection dynamics with the neighbouring subsystems, $\eta_x^{(I)} \in \mathbb{R}^{n_I - r_I}, \eta_z^{(I)} \in \mathbb{R}^{r_I}$ represent the system disturbances, $\xi^{(I)} : \mathbb{R}^{n_I} \times \mathbb{R}^{k_I} \times \mathbb{R}^{l_I} \mapsto \mathbb{R}^{n_I - r_I}$ is a smooth vector field.The term $A^{(I)}x^{(I)}$ represents the linear part of the system's $\Sigma^{(I)}$ dynamics, where $A^{(I)} \in \mathbb{R}^{(n_I - r_I) \times (n_I - r_I)}$ is assumed known.

Each system incorporates a set of sensors $\mathcal{S}^{(I)} = \bigcup_{j=1}^{n_I} \mathcal{S}^{(I)}\{j\}$ described as:

$$\mathcal{S}^{(I)}: \begin{cases} y_x^{(I)}(t) = x^{(I)}(t) + d_x^{(I)}(t) + f_x^{(I)}(t) \\ y_z^{(I)}(t) = z^{(I)}(t) + d_z^{(I)}(t) + f_z^{(I)}(t) \end{cases} \quad (2)$$

where $y_x^{(I)} \in \mathbb{R}^{n_I - r_I}$ denotes the sensor values corresponding to state variables, $y_z^{(I)} \in \mathbb{R}^{r_I}$ denotes the sensor values corresponding to algebraic variables, $d_x^{(I)} \in \mathbb{R}^{n_I - r_I}$, $d_z^{(I)} \in \mathbb{R}^{r_I}$ are the measurement noise vectors and $f_x^{(I)} \in \mathbb{R}^{n_I - r_I}$, $f_z^{(I)} \in \mathbb{R}^{r_I}$ are sensor fault vectors. Each fault vector is given by $f^{(I)}(t) = [f_x^{(I)}(t)\ f_z^{(I)}(t)]^\top = [f_1^{(I)}(t), \cdots, f_{n_I}^{(I)}(t)]^\top$, where $f_j^{(I)}(t), j \in \{1, \cdots, n_I\}$ denotes the sensor fault of the j-th sensor.

The objective of this paper is to design a methodology for the detection and isolation of multiple, permanent abrupt offset sensor faults for nonlinear DAE interconnected subsystems described by (1) and (2), subject to the following assumptions:

Assumption 1: The system disturbance and the measurement noise of each sensor are unknown but uniformly bounded, meaning: $\left|\eta_{xj}^{(I)}\right| \leqslant \overline{\eta}_{xj}^{(I)}$, $\left|\eta_{zj}^{(I)}\right| \leqslant \overline{\eta}_{zj}^{(I)}$, $\left|d_j^{(I)}\right| \leqslant \overline{d}_j^{(I)}, \forall j \in 1, \cdots, n_I$ where $\overline{\eta}_{xj}^{(I)}, \overline{\eta}_{zj}^{(I)}, \overline{d}_j^{(I)}$ are known.

Assumption 2: The nonlinear vector fields $\gamma^{(I)}, h^{(I)}$ are locally Lipschitz in $x \in \mathcal{X}$, $z \in \mathcal{Z}$ for all $u \in \mathcal{U}$ and $t \geqslant 0$ with Lipschitz constants λ_{γ_I}, λ_{h_I} respectively

3. FUEL ENGINE STATE-SPACE MODELLING

In order to describe the operation of the fuel engine, the physical MVFP model shown in [Geertsma et al. (2017)] is used. As shown in Fig. 1, the MVFP system model is decomposed in four nonlinear DAE interconnected subsystems, formulated using the general formulation shown in (1), (2). For simplicity purposes, the time dependence may hereby be omitted.

3.1 Fuel Pump ($\Sigma^{(1)}$)

Subsystem 1 is expressed as:

$$\Sigma^{(1)}: \dot{x}^{(1)} = -\frac{1}{\tau_X}x^{(1)} + \frac{x_{nom}^{(1)}}{\tau_X}u^{(1)} \quad (3)$$

where $x^{(1)}(t) \in \mathbb{R}$ is the amount of fuel injected per cylinder per engine cycle in kg, $x^{(1)}_{nom} \in \mathbb{R}$ signifies the same quantity under nominal conditions calculated as:

$$x^{(1)}_{nom} = \frac{SFC^{nom} P^{nom}_{fe} k_e}{i_e n^{nom}_{fe}} \tag{4}$$

, $u(t) \in \mathbb{R}$ is the fuel injection setting in % and n^{nom}_{fe}, $\tau_X = \frac{1}{4n^{nom}_{fe}}$, SFC^{nom}, P^{nom}_{fe}, i_e, k_e are defined in [Geertsma et al. (2017)]. The output of the fuel injection sensor $y^{(1)} \in \mathbb{R}$ is described by:

$$\mathcal{S}^{(1)} : y^{(1)} = x^{(1)}(t) + d^{(1)} + f^{(1)} \tag{5}$$

3.2 Thermomechanical process ($\Sigma^{(2)}$)

This subsystem has 3 algebraic variables, namely the pressure ($z^{(2)}_1$) in Pa and the temperature ($z^{(2)}_2$) in K inside the engine's cylinders and the engine's shaft torque ($z^{(2)}_3$) in Nm. The mathematical representation of the system is:

$$\Sigma^{(2)} : 0 = \begin{bmatrix} z^{(2)}_1 - \xi^{(2)}_{z1}(x^{(1)}, z^{(2)}_3, x^{(4)}, z^{(4)}_1) \\ z^{(2)}_2 - \xi^{(2)}_{z2}(x^{(1)}, z^{(2)}_3, x^{(4)}, z^{(4)}_1) \\ z^{(2)}_3 - \xi^{(2)}_{z3}(x^{(1)}, z^{(2)}_3, x^{(4)}, z^{(4)}_1) \end{bmatrix} \tag{6}$$

where the functions $\xi^{(2)}_{z1}, \xi^{(2)}_{z2}, \xi^{(2)}_{z3} \in \mathbb{R}$ can be modelled using the Seilinger thermodynamic cycle as follows[Geertsma et al. (2017)]:

$$\xi^{(2)}_{z1} = x^{(4)} r_c^{\kappa_a} \left(1 + \frac{\frac{1}{c_{v,a}} \left(X_{cv} \frac{\eta h_L R_a}{v_1} \frac{z^{(4)}_1}{x^{(4)}} x^{(1)} \right)}{z^{(4)}_1(t) r_c^{(\kappa_a - 1)}} \right) \cdot \left(\frac{r_{eo} r_c}{1 + \frac{(1 - X_{cv} - X_{ct}) \frac{\eta h_L R_a}{v_1} \frac{z^{(4)}_1}{x^{(4)}} x^{(1)}}{\left(z^{(4)}_1(t) r_c^{(\kappa_a - 1)} + \frac{X_{cv} \frac{\eta h_L R_a}{v_1} \frac{z^{(4)}_1}{x^{(4)}} x^{(1)}}{c_{v,a}} \right) c_{p,a}}} \right)^{-n_{exp}} \cdot e^{- \frac{(n_{exp} - 1) X_{ct} \frac{\eta h_L}{v_1} \frac{r_c^{(1-\kappa_a)}}{x^{(4)}} x^{(1)}}{1 + \frac{X_{cv} \frac{\eta h_L R_a}{v_1} \frac{r_c^{(1-\kappa_a)}}{x^{(4)}} x^{(1)}}{c_{v,a}} + \frac{(1 - X_{cv} - X_{ct}) \frac{\eta h_L R_a}{v_1} \frac{r_c^{(1-\kappa_a)}}{x^{(4)}} x^{(1)}}{c_{p,a}}}} \tag{7}$$

$$\xi^{(2)}_{z2} = \left(1 + \frac{\frac{\eta h_L R_a}{v_1} \frac{r_c^{(1-\kappa_a)}}{x^{(4)}} x^{(1)} \left(c_{p,a} X_{cv} + c_{v,a}(1 - X_{cv} - Xct) \right)}{c_{v,a} c_{p,a}} \right) \cdot \left(\frac{r_{eo} r_c (z^{(4)}_1 r_c^{(\kappa_a - 1)})^{(n_{exp} - 1)}}{1 + \frac{(1 - X_{cv} - X_{ct}) \frac{\eta h_L R_a}{v_1} \frac{z^{(4)}_1}{x^{(4)}} x^{(1)}}{\left(z^{(4)}_1(t) r_c^{(\kappa_a - 1)} + \frac{X_{cv} \frac{\eta h_L R_a}{v_1} \frac{z^{(4)}_1}{x^{(4)}} x^{(1)}}{c_{v,a}} \right) c_{p,a}}} \right)^{1 - n_{exp}} \cdot e^{\frac{(n_{exp} - 1) X_{ct} \frac{\eta h_L}{v_1} \frac{r_c^{(1-\kappa_a)}}{x^{(4)}} x^{(1)}}{1 + \frac{X_{cv} \frac{\eta h_L R_a}{v_1} \frac{r_c^{(1-\kappa_a)}}{x^{(4)}} x^{(1)}}{c_{v,a}} + \frac{(1 - X_{cv} - X_{ct}) \frac{\eta h_L R_a}{v_1} \frac{r_c^{(1-\kappa_a)}}{x^{(4)}} x^{(1)}}{c_{p,a}}}} \tag{8}$$

$$\xi^{(2)}_{z3} = \frac{v_1 i_e x^{(4)}}{2\pi k_e} \left(\frac{r_c^{(\kappa_a - 1)} - 1}{\kappa_a - 1} + \frac{(1 - X_{cv} - X_{ct})}{c_{p,a}} \frac{\eta h_L}{v_1} \frac{R_a}{x^{(4)}} x^{(1)} - \frac{r_c^{(\kappa_a - 1)} + \frac{\frac{\eta h_L R_a}{v_1 x^{(4)}} x^{(1)} (c_{p,a} X_{cv} + c_{v,a}(1 - X_{cv} - Xct))}{c_{v,a} c_{p,a}}}{n_{exp} - 1} + \frac{X_{ct} \eta h_L R_a x^{(1)}}{x^{(4)} v_1} + \frac{\xi^{(2)}_{z2}}{z^{(4)}_1 (n_{exp} - 1)} \right) - Q^{nom}_{loss} \left(1 + Q^{grad}_{loss} \cdot \frac{n^{nom}_{fe} - n_{fe}}{n^{nom}_{fe}} \right) \tag{9}$$

where $n_{fe} = \sqrt{\frac{2\pi}{c} z^{(2)}_3}$, $X_{cv} = X^{nom}_{cv} + X^{grad}_{cv} \frac{n_{fe} - n^{nom}_{fe}}{n^{nom}_{fe}}$, $X_{ct} = X^{nom}_{ct} \frac{x^{(1)}}{x^{(1)}_{nom}}$, c is a constant, η is the thermal efficiency incorporating both the combustion and heat release processes and X^{nom}_{cv}, X^{grad}_{cv}, X^{nom}_{ct}, h_L, R_a, v_1, r_c, κ_a, r_{eo}, n_{exp}, $c_{p,a}$, $c_{v,a}$, Q^{nom}_{loss}, Q^{grad}_{loss} are defined in [Geertsma et al. (2017)]. The output values of the pressure, temperature and torque sensors $y^{(2)} \in \mathbb{R}^3$ are described by:

$$\mathcal{S}^{(2)} : y^{(2)} = z^{(2)} + d^{(2)} + f^{(2)} \tag{10}$$

3.3 Exhaust Gas Path ($\Sigma^{(3)}$)

This subsystem has 1 state-variable, the exhaust receiver pressure ($x^{(3)}$) in Pa and 2 algebraic variables, the temperature before ($z^{(3)}_1$) and after ($z^{(3)}_2$) the turbine in K. This subsystem is represented as follows in state-space:

$$\Sigma^{(3)} : \begin{cases} \dot{x}^{(3)} = -\frac{1}{\tau_{p_d}} x^{(3)} + h^{(3)}(x^{(3)}, z^{(3)}, \chi^{(3)}) \\ 0 = \quad \xi^{(3)}(x^{(3)}, z^{(3)}, \chi^{(3)}) \end{cases} \tag{11}$$

where $\chi^{(3)} = [x^{(1)}, z^{(2)}, x^{(4)}, z^{(4)}]^\top$ are the interconnection variables. The interconnection dynamics are described by

$$h^{(3)}(x^{(3)}, z^{(3)}, \chi^{(3)}) = \frac{1}{\tau_{p_d}} \sqrt{p^2_{ex} + \frac{z^{(3)}_1 (n^2_{fe} \left(\psi_1 \frac{x^{(4)}}{z^{(4)}_1} + \frac{i_e}{k_e} x^{(1)} \right)^2}{a^2_Z A_{eff}}} \tag{12}$$

where $\psi_1 = \psi_1(x^{(3)}, x^{(4)}, z^{(4)}, n_{fe}) = \frac{\sqrt{R_g} i_e v_1 s_{sl}(x^{(3)}, x^{(4)}, z^{(4)}, n_{fe})}{R_a k_e}$. The algebraic part is expressed as

$$\xi^{(3)}(x^{(3)}, z^{(3)}, \chi^{(3)})) = \begin{bmatrix} z^{(3)}_1 - \frac{\psi_2 T_{sl} + \widetilde{\psi}_3 z^{(2)}_2}{\psi_2 + \psi_3} \\ z^{(3)}_2 - \psi_4 z^{(3)}_1 \end{bmatrix} \tag{13}$$

where

$$\psi_2 = \frac{c_{pa} v_1 s_{sl}(x^{(3)}, x^{(4)}, z^{(4)}, z^{(2)}) \frac{x^{(4)}}{z^{(4)}_1}}{R_a} \tag{14}$$

$$\psi_3 = c_{pg} \left(x^{(1)} + \frac{v_1}{R_a} \frac{x^{(4)}}{z^{(4)}_1} \right) \tag{15}$$

$$\widetilde{\psi}_3 = \psi_3(t) \left(\frac{1}{n_{bld}} + \frac{n_{bld} - 1}{n_{bld}} \tau_{p_d} \frac{h^{(3)}}{z^{(2)}_1} \right) \tag{16}$$

$$\psi_4 = 1 + \eta_{tur}(x^{(4)}) (\Pi_{tur} - 1) \tag{17}$$

$$\Pi_{tur} = \Pi_{tur}(x^{(3)}) = \left(\frac{p_{ex}}{x^{(3)}} \right)^{(\frac{\kappa_g - 1}{\kappa_g})} \tag{18}$$

$$\eta_{tur}(x^{(4)}) = a_{tur} + b_{tur} x^{(4)} + c_{tur} (x^{(4)})^2 \tag{19}$$

and $\tau_{p_d}, p_{ex}, a_Z, A_{eff}, R_g, n_{bld}, \kappa_g\, c_{pg}, T_{sl}, a_{tur},\ b_{tur},\ c_{tur}$ s_{sl} are defined in [Geertsma et al. (2017)]. The related set of sensors is expressed as:

$$\mathcal{S}^{(3)} : y^{(3)} = \begin{bmatrix} x^{(3)} & z^{(3)} \end{bmatrix}^\top + d^{(3)} + f^{(3)} \tag{20}$$

3.4 Air Path ($\Sigma^{(4)}$)

This subsystem has 1 state-variable, the charge air pressure after the compressor ($x^{(4)}$) in Pa and 2 algebraic variables, the temperatures before ($z_1^{(4)}$) and after ($z_2^{(4)}$) the intercooler in K. This subsystem is represented as follows in state-space:

$$\Sigma^{(4)}: \begin{cases} \dot{x}^{(4)} = -\dfrac{1}{\tau_{TC}} x^{(4)} + h^{(4)}(x^{(4)}, z^{(4)}, \chi^{(4)}) \\ 0 = \quad \xi^{(4)}(x^{(4)}, z^{(4)}, \chi^{(4)}) \end{cases} \tag{21}$$

where $\chi^{(4)} = [x^{(1)}, z^{(2)}, x^{(3)}, z^{(3)}]^\top$ are the interconnection variables. The interconnection dynamics are expressed as:

$$h^{(4)} = \frac{p_{amb}}{\tau_{TC}} \left(1 + \chi_g \delta_f \eta_{TC}(x^{(4)}) r_{TC}(z^{(3)})(1 - \Pi_{tur})\right)^{\left(\frac{\kappa_a - 1}{\kappa_a}\right)} \tag{22}$$

where

$$\delta_f = 1 + \frac{x^{(1)}}{\left(1 + \frac{v_1}{R_a} s_{sl} \frac{x^{(4)}}{z_1^{(4)}}\right)} \tag{23a}$$

$$\eta_{TC}(x^{(4)}) = a_\eta + b_\eta x^{(4)} + c_\eta (x^{(4)})^2 \tag{23b}$$

$$r_{TC}(z^{(3)}) = \frac{z_1^{(3)}}{T_{amb}} \tag{23c}$$

The algebraic part is described by

$$\xi^{(4)}(x^{(4)}, z^{(4)}, \chi^{(4)})) = \begin{bmatrix} z_1^{(4)} - \xi_{z1}^{(4)} \\ z_2^{(4)} - \xi_{z2}^{(4)}(x^{(3)}, z^{(3)}) \end{bmatrix} \tag{24}$$

where

$$\xi_{z1}^{(4)} = T_c - \epsilon_{inl}(T_{inl} - T_c) \tag{25a}$$

$$\xi_{z2}^{(4)} = T_{amb} + \chi_g \eta_{tur}(\delta_f(t) + \eta_{com}) x^{(3)} \left(z_2^{(3)} - z_1^{(3)}\right) \tag{25b}$$

and τ_{TC}, χ_g, p_{amb}, T_{amb}, a_η, b_η, c_η, η_{com}, T_c, ϵ_{inl}, T_{inl} are defined in [Geertsma et al. (2017)]. The sensor set of this system is given by:

$$\mathcal{S}^{(4)}: y^{(4)} = \begin{bmatrix} x^{(4)} & z^{(4)} \end{bmatrix}^\top + d^{(4)} + f^{(4)} \tag{26}$$

4. DISTRIBUTED SENSOR FAULT DETECTION AND ISOLATION

Due to the large scale of marine fuel engines as well as their inherent system complexity, a distributed monitoring approach is proposed. As shown in Fig. 2, for each one of the fuel engine's subsystems $\Sigma^{(I)}$, $I = 1, \cdots, N$ (N=4), a monitoring agent $\mathcal{M}^{(I)}$ is designed consisting of N_I modules $\mathcal{M}^{(I,q)}$, $q = 1, \cdots, N_I$ ($N_1 = 1$, $N_2 = N_3 = N_4 = 3$). Each module monitors a specific sensor subset $\mathcal{S}^{(I,q)} \subseteq \mathcal{S}^{(I)}$ in the designated subsystem. Every $\mathcal{S}^{(I,q)}$ contains sensors measuring either state or algebraic variables.

Remark 1: The distributed scheme in Fig.2 is based on previous works [e.g. Reppa et al. (2016)]. However, the monitoring agents $\mathcal{M}^{(I)}$, $I = \{1, 2, 3, 4\}$ have been designed considering the DAE nature of the fuel engine system. In more detail, nonlinear algebraic residuals with corresponding adaptive bounds were proposed.

4.1 Residual generation

The residual vector $\epsilon_y^{(I,q)} \in \mathbb{R}^{n_I}$ is defined by:

$$\epsilon_y^{(I,q)} = \begin{bmatrix} y_x^{(I,q)} - \hat{x}^{(I,q)} \\ -\xi^{(I)}(y_x^{(I,q)}, y_z^{(I,q)}, y_\chi^{(I)}, u^{(I)}) \end{bmatrix} = \begin{bmatrix} \epsilon_{y_x}^{(I,q)} \\ \epsilon_{y_z}^{(I,q)} \end{bmatrix} \tag{27}$$

where $\hat{x}^{(I,q)}$ is the estimation of $x^{(I)}$ defined as:

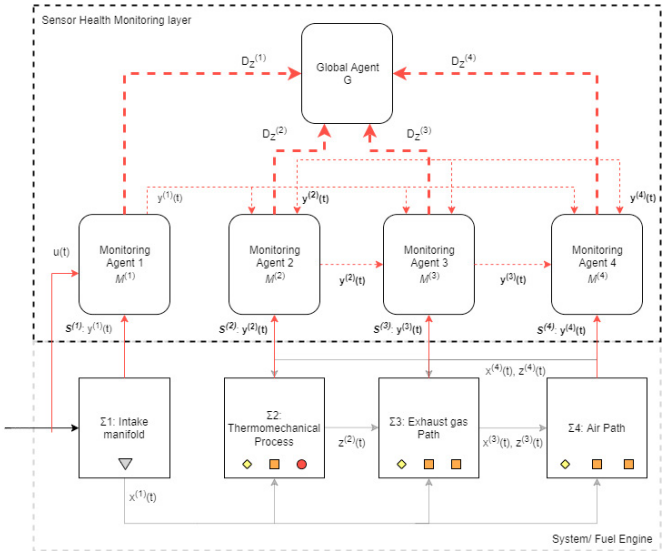

Fig. 2. Distributed SFDI scheme application using a MVFP Fuel Engine model

$$\begin{aligned} \dot{\hat{x}}^{(I,q)}(t) =& A^{(I)}\hat{x}^{(I,q)}(t) + \gamma^{(I)}(\hat{x}^{(I,q)}(t), y_z^{(I,q)}(t), u^{(I)}(t)) \\ &+ h^{(I)}(\hat{x}^{(I,q)}(t), y_z^{(I,q)}(t), y_\chi^{(I)}(t), u^{(I)}(t)) \\ &+ L^{(I,q)}(y_x^{(I,q)}(t) - \hat{x}^{(I,q)}(t)), \end{aligned} \tag{28}$$

The matrix $L^{(I,q)} \in \mathbb{R}^{(n_I - r_I)\times(n_I - r_I)}$ is chosen such that the matrix $A_L^{(I,q)} = A^{(I)} - L^{(I,q)}$ is Hurwitz.

Subtracting (1) from (28) and using (2) yields:

$$\dot{\epsilon}_x^{(I,q)} = A_L^{(I,q)}\epsilon_x^{(I,q)} + \tilde{\gamma}^{(I,q)} + \tilde{h}^{(I,q)} + \eta_x^{(I)} - L^{(I,q)} d_x^{(I,q)} \tag{29}$$

where $\epsilon_x^{(I,q)} = x^{(I)} - \hat{x}^{(I,q)}$ is the state estimation error, $\tilde{\gamma}^{(I,q)} \triangleq \gamma^{(I)}(x^{(I)}(t), z^{(I)}(t), u^{(I)}(t)) - \gamma^{(I)}(\hat{x}^{(I,q)}(t), y_z^{(I,q)}(t), u^{(I)}(t))$ and $\tilde{h}^{(I,q)} = h^{(I)}(x^{(I)}(t), z^{(I)}(t), \chi^{(I)}(t), u^{(I)}(t)) - h^{(I)}(\hat{x}^{(I,q)}(t), y_z^{(I,q)}(t), y_\chi^{(I)}(t), u^{(I)}(t))$. The residual $\epsilon_{y_x}^{(I,q)}$ can then also be expressed as $\epsilon_{y_x}^{(I,q)} = \epsilon_x^{(I,q)} + d_x^{(I,q)}$

Adding (1b) to the expression of $\epsilon_{y_z}^{(I,q)}$ in (27) yields:

$$\begin{aligned} \epsilon_{y_z}^{(I,q)}(t) =& \xi^{(I)}(x^{(I)}, z^{(I)}, \chi^{(I)}, u^{(I)}) + \eta_z^{(I)} \\ &- \xi^{(I)}(y_x^{(I,q)}, y_z^{(I,q)}, y_\chi^{(I)}, u^{(I)}) \end{aligned} \tag{30}$$

4.2 Adaptive thresholds' computation

The thresholds are designed to bound the respective residuals $\epsilon_{y_x}^{(I,q)}$ and $\epsilon_{y_z}^{(I,q)}$ under healthy sensor conditions. This translates to the following requirements for the adaptive threshold(s) of the j-th component of the residual vector:

$$\left|\epsilon_{y_{x_j}}^{(I,q)}(t)\right| \leq \bar{\epsilon}_{y_{x_j}}^{(I,q)}(t), \; j = 1, \cdots, n_I - r_I \tag{31}$$

$$\epsilon_{y_{z_j}}^{(I,q)}(t) \in [\underline{\epsilon}_{y_{z_j}}^{(I,q)}(t), \bar{\epsilon}_{y_{z_j}}^{(I,q)}(t)], \; j = 1, \cdots, r_I \tag{32}$$

Adaptive thresholds in (31),(32) are designed considering the Assumptions 1 and 2. This design causes no false alarms. Under the Assumptions 1-2 and after some mathematical manipulations of (29) the adaptive threshold can be computed as [Reppa et al. (2016)]:

$$\bar{\epsilon}_{y_{x_j}}^{(I,q)}(t) = E^{(I,q)}(t) + \rho^{(I,q)}\Lambda_I \int_0^t E^{(I,q)}(\tau) e^{-\xi^{(I,q)}(t-\tau)} \, d\tau + \bar{d}_{x_j}^{(I,q)} \tag{33}$$

$$E^{(I,q)}(t) = \rho^{(I,q)} e^{-\xi^{(I,q)}t}\bar{x}^{(I,q)} + \frac{\rho_d^{(I,q)}\bar{d}_x^{(I,q)}}{\xi_d^{(I,q)}}(1-e^{-\xi_d^{(I,q)}t}) + \frac{\rho^{(I,q)}\lambda_{h_I}\bar{d}_\chi^{(I)}}{\xi^{(I,q)}}(1-e^{-\xi^{(I,q)}t}) \quad (34)$$

where $\Lambda_I = \lambda_{h_I} + \lambda_{\gamma_I}$, $\rho^{(I,q)}, \xi^{(I,q)}, \rho_d^{(I,q)}, \xi_d^{(I,q)}$ are positive constants such that $\left|e^{A_L^{(I,q)}t}\right| \leqslant \rho^{(I,q)}e^{-\xi^{(I,q)}t}$ and $\left|e^{A_L^{(I,q)}t}L^{(I,q)}\right| \leqslant \rho_d^{(I,q)}e^{-\xi_d^{(I,q)}t}$. For the algebraic thresholds, inclusion functions can be used to calculate the thresholds [Jaulin and Walter (1993)]. Given that $[x^{(I)}] = y_x^{(I,q)} + [d_x^{(I,q)}]$ ($[x_j^{(I)}] = [y_{x_j}^{(I,q)} - \bar{d}_{x_j}^{(I,q)}, y_{x_j}^{(I,q)} + \bar{d}_{x_j}^{(I,q)}] = y_{x_j}^{(I,q)} + [d_{x_j}^{(I,q)}]$, $j = 1, \cdots, n_I - r_I$), $[z^{(I)}] = y_z^{(I,q)} + [d_z^{(I,q)}]$, $[\chi^{(I)}] = y_\chi^{(I)} + [d_\chi^{(I)}]$,$[u^{(I)}] = [\underline{u}^{(I)}, \bar{u}^{(I)}]$ it can be deduced that:

$$\xi_j^{(I)}(x^{(I)}, z^{(I)}, \chi^{(I)}, u^{(I)}) \in [\underline{\xi}_j^{(I)}, \bar{\xi}_j^{(I)}] \quad (35)$$

where $[\underline{\xi}_j^{(I)}, \bar{\xi}_j^{(I)}] = \xi_j^{(I)}(y_x^{(I,q)} + [d_x^{(I,q)}], y_z^{(I,q)} + [d_z^{(I,q)}], y_\chi^{(I)} + [d_\chi^{(I)}], [u^{(I)}])$. Then, according to (30) and Assumption 1:

$$\begin{cases} \underline{\epsilon}_{y_{z_j}}^{(I,q)} = \underline{\xi}_j^{(I)} - \xi_j^{(I)}(y_x^{(I,q)}, y_z^{(I,q)}, y_\chi^{(I)}, u^{(I)}) \\ \bar{\epsilon}_{y_{z_j}}^{(I,q)} = \bar{\xi}_j^{(I)} - \xi_j^{(I)}(y_x^{(I,q)}, y_z^{(I,q)}, y_\chi^{(I)}, u^{(I)}) \end{cases} \quad (36)$$

Remark 2: The conservativeness of the design of the adaptive algebraic thresholds using interval analysis in (36) depends on the nonlinearity of the system

4.3 Multiple sensor Fault Decision Logic

This section describes the multiple sensor fault decision logic. As shown in Fig. 2, isolation occurs in two steps; the local and global decision logic [Reppa et al. (2016)].

Local decision Logic The presence of faults in $\mathcal{S}^{(I,q)}$ is detected by the modules $\mathcal{M}^{(I,q)}$ based on a set of analytical redudancy relations (ARRs). The j-th ARR is defined as:

$$\mathcal{E}_j^{(I,q)} : \left|\epsilon_{y_{x_j}}^{(I,q)}(t)\right| - \bar{\epsilon}_{y_{x_j}}^{(I,q)}(t) \leqslant 0,\ j = 1, \cdots, n_I - r_I \quad (37)$$

for the monitoring modules using the residual expression $\epsilon_{y_x}^{(I,q)}$ defined in (27) and the threshold expression of (33). Otherwise, the j-th ARR is defined as follows:

$$\mathcal{E}_j^{(I,q)} : \epsilon_{y_{z_j}}^{(I,q)}(t) \in [\underline{\epsilon}_{y_{z_j}}^{(I,q)}(t), \bar{\epsilon}_{y_{z_j}}^{(I,q)}(t)],\ j = 1, \cdots, r_I \quad (38)$$

The set of ARRs based on which the module decides on the presence of local sensor faults is defined as $\mathcal{E}^{(I,q)} = \bigcup_{j\in\mathcal{J}^{(I,q)}} \mathcal{E}_j^{(I,q)}$, where $\mathcal{J}^{(I,q)}$ is an index set.

The first time instant that (37) or (38) is invalid for at least one $j \in \mathcal{J}^{(I,q)}$ signifies the time instant of fault detection $T_{D_j}^{(I,q)}$ by the local SFDI module $\mathcal{M}^{(I,q)}$, defined as $T_{D_j}^{(I,q)} = \min\{t : \left|\epsilon_{y_{x_j}}^{(I,q)}(t)\right| - \bar{\epsilon}_{y_{x_j}}^{(I,q)}(t) > 0\}$ or $T_{D_j}^{(I,q)} = \min\{t : \epsilon_{y_{z_j}}^{(I,q)}(t) \notin [\underline{\epsilon}_{y_{z_j}}^{(I,q)}(t), \bar{\epsilon}_{y_{z_j}}^{(I,q)}(t)]\}$ accordingly. Until this instant, the local sensing subsystem $\mathcal{S}^{(I,q)}$ is considered non-faulty meaning that either no fault exists or that faults exist but remain undetected.

The output of $\mathcal{M}^{(I,q)}$ is denoted by $D^{(I,q)}$ and in the case of permanent sensor faults, it can be defined as:

$$D^{(I,q)}(t) = \begin{cases} 0 & , t < T_D^{(I,q)} \\ 1 & , t \geqslant T_D^{(I,q)} \end{cases} \quad (39)$$

with $T_D^{(I,q)} = \min\{T_{D_j}^{(I,q)} : j \in \mathcal{J}^{(I,q)}\}$.

Thus, a binary decision vector $D^{(I)} = [D^{(I,1)}, \cdots, D^{(I,N_I)}]$ can be obtained for the monitoring agent $\mathcal{M}^{(I)}$ and compared to the columns of a binary fault signature matrix $F^{(I)}$, consisting of N_I rows and $N_{C_I} + 2$ columns where $N_{C_I} = 2^{n_I} - 1$. The design of this matrix will be described in the simulation results section for the easiness of the analysis. While $D^{(I)}(t) = 0_{N_I}$, the diagnosis set $\mathcal{D}_s^{(I)}$ is empty. In addition, if $D^{(I,q)} = F_{qi}^{(I)}\ \forall q \in 1, \cdots, N_I$, then the observed pattern $\mathcal{D}^{(I)}(t)$ is said to be consistent with the theoretical pattern $F_i^{(I)}$ and the diagnosis set is defined as $\mathcal{D}_s^{(I)}(t) = \{\mathcal{F}_{ci}^{(I)} : i \in \mathcal{I}_\mathcal{D}^{(I)}(t)\}$ where $\mathcal{I}_\mathcal{D}^{(I)}(t)$ is the consistency index set defined as $\mathcal{I}_\mathcal{D}^{(I)}(t) = \{i : F_i^{(I)} = D^{(I)}(t), i \in \{1, \cdots, N_{C_I}\}\}$. The agent $\mathcal{M}^{(I)}, I \in \{1, \cdots, N\}$ also provides a decision on the propagation of sensor faults from the interconnected subsystems, denoted as $D_\chi^{(I)}(t)$ with

$$D_\chi^{(I)}(t) = \begin{cases} 0 & , \text{if } f_\chi^{(I)} \notin \mathcal{D}_s^{(I)}(t) \text{ and } f_p^{(I)} \notin \mathcal{D}_s^{(I)}(t) \\ 1 & , \text{otherwise} \end{cases} \quad (40)$$

where $f_p^{(I)} \in \mathbb{R}^{n_I^*}, n_I^* \leqslant n_I$, collectively amounts for the sensor faults that are propagated from the agent $\mathcal{M}^{(I)}$ to its neighbouring agents due to the exchange of sensor information and $f_\chi^{(I)}$ corresponds to the sensor faults propagated to the agent from the neighbouring agents.

Global Decision Logic The global decision logic serves to isolate sensor faults propagated through the interconnections between the monitoring agents. As shown in Fig.2, a global agent $\mathcal{G}$ collects the decisions on the propagation of sensor faults from the N local agents $D_\chi(t) = [D_\chi^{(1)}(t), \cdots, D_\chi^{(N)}(t)]$ and compares them with the columns of a global binary sensor fault signature matrix F^χ consisting of N rows and $N_C = 2^p - 1$ columns ($p \leqslant \sum_{I=1}^N \{p_I\}$, p_I is the length of $f_\chi^{(I)}$). If $\mathcal{D}_\chi(t)$ is consistent with the k-th column of F^χ (F_k^χ), the diagnosis set of propagated sensor faults is defined as $\mathcal{D}_s^\chi(t) = \{\mathcal{F}_{ck}^\chi : k \in \mathcal{I}_\chi(t)\}$, where $\mathcal{I}_\chi(t)$ is an index set defined as $\mathcal{I}_\chi(t) = \{k : F_{Ik}^\chi = D_\chi^{(I)}(t), k \in \{1, \cdots, N_C\}, \forall I \in \{1, \cdots, N\}\}$.

The set $\mathcal{D}_s^\chi(t)$ is then used to update the non-empty local diagnosis set $\mathcal{D}_s^{(I)}(t)$ of $\mathcal{M}^{(I)}$ by excluding the occurrence of $f_\chi^{(I)}$ and its combinations, if $f_\chi^{(I)} \notin \mathcal{D}_s^\chi(t)$. Thus, the global diagnosis set can be expressed as $\mathcal{D}_s^\mathcal{G}(t) = \mathcal{D}_s^\chi \bigcap_{\mathcal{D}_s^{(I)}\neq\emptyset}^{N_{I=1}} \mathcal{D}_s^{(I)}$

5. SIMULATION RESULTS

In this section, we apply the Distributed SFDI architecture described in Section 4 in the case of a Diesel Engine using data from Geertsma et al. (2017) and the state-space modelling of the different interconnected subsystems shown in Section 3. It is assumed that the measurements of each sensor of the engine are corrupted by uniformly distributed noise equal to 3% of the amplitude of the noiseless measurements of the sensor.

The 10 sensors of the system are divided in the following sensor sets: $\mathcal{S}^{(1,1)} = \{\mathcal{S}^{(1)}\{1\}\}$, $\mathcal{S}^{(2,1)} = \{\mathcal{S}^{(2)}\{1\}\}$,

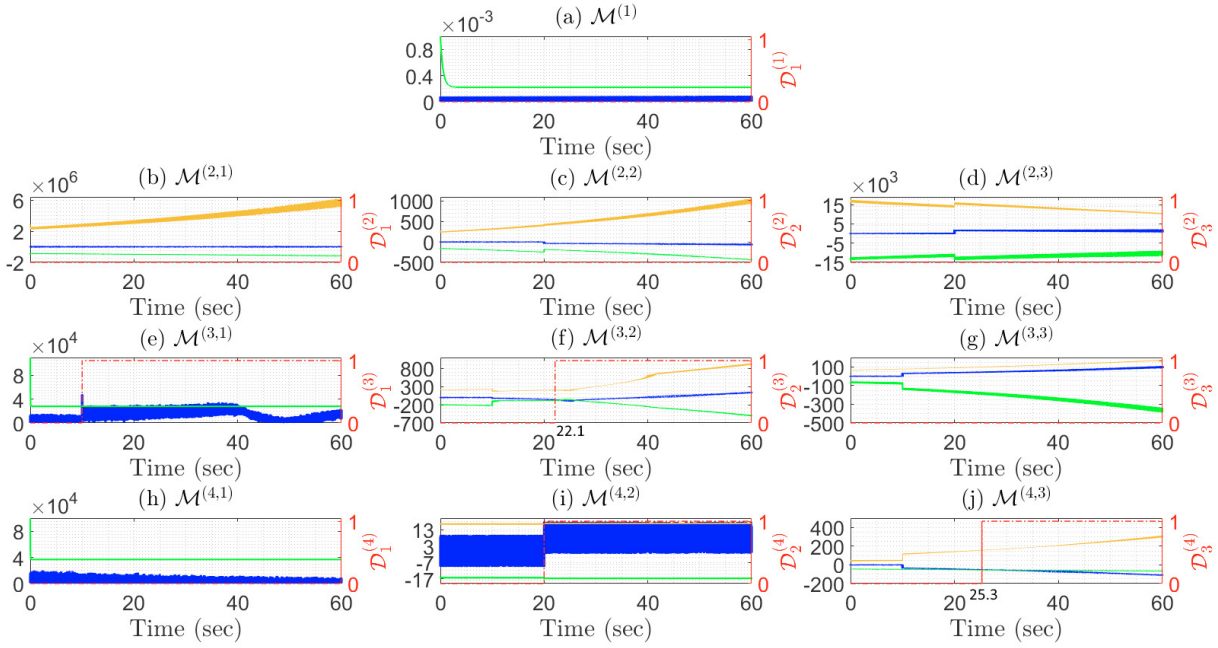

Fig. 3. Simulation results of the Distributed SFDI methodology for the specified fault scenario (red line: decision logic, blue line: residual, green and orange lines: adaptive thresholds)

Table 1. Part of the Sensor Fault signature matrix of $\mathcal{M}^{(3)}$ (*:0 or 1)

	$f_1^{(3)}$	$f_2^{(3)}$	$f_3^{(3)}$	$f_1^{(1)}$	$f_1^{(2)}$	$f_2^{(2)}$	$f_3^{(2)}$	$f_1^{(4)}$	$f_2^{(4)}$
$\mathcal{E}^{(3,1)}$	1	1	0	*	0	0	*	*	*
$\mathcal{E}^{(3,2)}$	*	*	0	*	*	*	*	*	*
$\mathcal{E}^{(3,3)}$	*	*	*	0	0	0	0	0	0

Table 2. Part of the Sensor Fault signature matrix of $\mathcal{M}^{(4)}$ (*:0 or 1)

	$f_1^{(4)}$	$f_2^{(4)}$	$f_3^{(4)}$	$f_1^{(1)}$	$f_3^{(2)}$	$f_1^{(3)}$	$f_2^{(3)}$
$\mathcal{E}^{(4,1)}$	1	1	0	*	*	*	*
$\mathcal{E}^{(4,2)}$	0	*	0	0	0	0	0
$\mathcal{E}^{(4,3)}$	*	*	*	*	*	*	*

Table 3. Part of the Global sensor fault signature matrix (*:0 or 1)

	$f_1^{(1)}$	$f_1^{(2)}$	$f_2^{(2)}$	$f_3^{(2)}$	$f_1^{(3)}$	$f_2^{(3)}$	$f_3^{(3)}$	$f_1^{(4)}$	$f_2^{(4)}$	$f_3^{(4)}$
$\mathcal{E}^{(1)}$	1	0	0	0	0	0	0	0	0	0
$\mathcal{E}^{(2)}$	*	1	1	1	0	0	0	*	*	0
$\mathcal{E}^{(3)}$	*	*	*	*	1	1	1	*	*	0
$\mathcal{E}^{(4)}$	*	0	0	*	*	*	0	1	1	1

$\mathcal{S}^{(2,2)} = \{\mathcal{S}^{(2)}\{2\}\}$, $\mathcal{S}^{(2,3)} = \{\mathcal{S}^{(2)}\{2\}, \mathcal{S}^{(2)}\{3\}\}$, $\mathcal{S}^{(3,1)} = \{\mathcal{S}^{(3)}\{1\}, \mathcal{S}^{(3)}\{2\}\}$, $\mathcal{S}^{(3,2)} = \{\mathcal{S}^{(3)}\{1\}, \mathcal{S}^{(3)}\{2\}\}$, $\mathcal{S}^{(3,3)} = \{\mathcal{S}^{(3)}\{1\}, \mathcal{S}^{(3)}\{2\}, \mathcal{S}^{(3)}\{3\}\}$, $\mathcal{S}^{(4,1)} = \{\mathcal{S}^{(4)}\{1\}, \mathcal{S}^{(4)}\{2\}\}$, $\mathcal{S}^{(4,2)} = \{\mathcal{S}^{(4)}\{2\}\}$, $\mathcal{S}^{(4,3)} = \{\mathcal{S}^{(4)}\{2\}, \mathcal{S}^{(4)}\{3\}\}$. Each of the modules $\mathcal{M}^{(I,q)}$ is then designed to use the information from the respective sensors in $\mathcal{S}^{(I,q)}$. The modules $\mathcal{M}^{(1,1)}$, $\mathcal{M}^{(3,1)}$ and $\mathcal{M}^{(4,1)}$ internally use an ARR expression of the form given in (37) while all the other modules use an ARR expression of the form given in (38). The index sets are defined as follows: $\mathcal{J}^{(1,1)} = \{1\}$, $\mathcal{J}^{(2,1)} = \{1\}$, $\mathcal{J}^{(2,2)} = \{2\}$, $\mathcal{J}^{(2,3)} = \{3\}$, $\mathcal{J}^{(3,1)} = \{1\}$, $\mathcal{J}^{(3,2)} = \{1\}$, $\mathcal{J}^{(3,3)} = \{2\}$, $\mathcal{J}^{(4,1)} = \{1\}$, $\mathcal{J}^{(4,2)} = \{1\}$, $\mathcal{J}^{(4,3)} = \{2\}$.

The design parameters of the various monitoring modules, introduced in Section 4, are selected as follows: $L^{(1,1)} = 1.16$, $\rho^{(1,1)} = 3$, $\xi^{(1,1)} = 2$, $\rho_d^{(1,1)} = 10$, $\xi_d^{(1,1)} = 2$, $L^{(3,1)} = 445$, $\rho^{(3,1)} = 1$, $\xi^{(3,1)} = 541$, $\rho_d^{(3,1)} = 465$, $\xi_d^{(3,1)} = 2$, $L^{(4,1)} = 319.98$, $\rho^{(4,1)} = 1$, $\xi^{(4,1)} = 301$, $\rho_d^{(4,1)} = 320$ and $\xi_d^{(4,1)} = 1$. The engine is simulated for 60 sec at its nominal operation point. A permanent abrupt offset sensor fault is assumed for the pressure sensor $\mathcal{S}^{(3)}\{1\}$ and the temperature sensor $\mathcal{S}^{(4)}\{2\}$. The fault magnitudes are $\widehat{\phi}_1^{(3)} = 5 \cdot 10^4 Pa$ and $\widehat{\phi}_2^{(4)} = 8K$ and their times of occurrence at $T_{f1}^{(3)} = 10\ sec$ and $T_{f2}^{(4)} = 20\ sec$.

Fig. 3 illustrates the results of the Distributed SFDI methodology for the considered fault scenario. As can be seen, the residuals, adaptive thresholds and local decisions are portrayed for each module of the different monitoring agents. Agents $\mathcal{M}^{(1)}, \mathcal{M}^{(2)}$ output zero decision vectors, as illustrated in Fig.3(a)-(d). The local sensor fault signature matrices for the monitoring agents $\mathcal{M}^{(3)}, \mathcal{M}^{(4)}$ are given in Tables 1,2 while Table 3 corresponds to the global decision matrix. Due to limited space, only the single fault signatures are provided.

In Table 1 the three first columns represent the single local sensor fault signatures while the rest of the columns portray the propagated sensor fault signatures from the neighbouring subsystems. As for the rows of this matrix, each of them corresponds to a local module $\mathcal{M}^{(3,q)}$ making use of the set of ARRs $\mathcal{E}^{(3,q)}$, $q = \{1, 2, 3\}$. A (*) is used instead of 1 in order to differentiate the sensitivity of the

different ARRs in case of local and propagated sensor faults and in case of algebraic and state-based ARRs. A similar approach is followed for the creation of Table 2.

For $t < 10$ *sec*, the diagnosis set is empty ($\mathcal{D} = \{\}$). For $10 \leqslant t < 20$ *sec*, the agents $\mathcal{M}^{(3)}$ and $\mathcal{M}^{(4)}$ produce the decision vectors $D^{(3)}(t) = [1\ 0\ 0]^\top$ and $D^{(4)}(t) = [0\ 0\ 0]^\top$ respectively, as can be seen in Fig.3(e)-(j). Thus, using Tables 1- 2, the resulting local diagnosis sets are $\mathcal{D}_s^{(3)}(t) = \{f_1^{(3)}, f_2^{(3)}, f_1^{(1)}, f_3^{(2)}, f_1^{(4)}, f_2^{(4)}, \{f_1^{(2)}, f_{j(I)}^{(I)}\}, \{f_2^{(2)}, f_{j(I)}^{(I)}\}, \{f_1^{(3)}, f_1^{(1)}\}, \{f_1^{(3)}, f_3^{(2)}\}, \cdots\}$, $I = 1, 2, 3, 4$, $j = \{1, \{\}, \{1, 2\}, \{1, 2\}\}$ and $\mathcal{D}_s^{(4)}(t) = \{\}$ respectively. The global decision vector is $D_\chi(t) = [0\ 0\ 1\ 0]^\top$ and when compared to Table 3, results in the diagnosis set on fault propagation $\mathcal{D}_s^\chi(t) = \{f_1^{(3)}, f_2^{(3)}, f_3^{(3)}\}$. Thus, the global diagnosis set is $\mathcal{D}_s^\mathcal{G}(t) = \mathcal{D}_s^\chi \cap \mathcal{D}_s^{(3)} = \{f_1^{(3)}, f_2^{(3)}\}$. For $20 \leqslant t < 22.1$ *sec*, the monitoring agent $\mathcal{M}^{(4)}$ outputs the decision vector $D^{(4)} = [0\ 1\ 0]^\top$ as shown in Fig. 3(h)-(j). According to Table 2, the new local diagnosis set for agent $\mathcal{M}^{(4)}$ is $\mathcal{D}_s^{(4)} = f_2^{(4)} \cup \{\{\}, f_1^{(1)}, f_3^{(2)}, f_1^{(3)}, f_2^{(3)}, \{f_1^{(1)}, f_3^{(2)}\}, \{f_1^{(1)}, f_1^{(3)}\}, \{f_1^{(1)}, f_2^{(3)}\}, \{f_3^{(2)}, f_1^{(3)}\}, \{f_3^{(2)}, f_2^{(3)}\}, \{f_1^{(1)}, f_3^{(2)}, f_1^{(3)}\}, \{f_1^{(1)}, f_3^{(2)}, f_2^{(3)}\}\}$. In addition, $\mathcal{D}_s^{(3)}$ remains the same since the decision vector of the agent $\mathcal{M}^{(3)}$ is the same (see Fig.3(e)-(g)) The minimum local diagnosis set is $\mathcal{D}_s(t) = \mathcal{D}_s^{(3)} \cap \mathcal{D}_s^{(4)} = \mathcal{D}_s^{(4)}$. Consulting the global decision vector $D_\chi(t) = [0\ 0\ 1\ 1]^\top$ and using Table 3, the diagnosis set on fault propagation is $\mathcal{D}_s^\chi = \{f_1^{(3)}, f_2^{(3)}, f_1^{(4)}, f_2^{(4)}, \{f_1^{(3)}, f_1^{(4)}\}, \{f_1^{(3)}, f_2^{(4)}\}, \{f_2^{(3)}, f_1^{(4)}\}, \{f_2^{(3)}, f_2^{(4)}\}\}$. As a result, for $20 \leqslant t < 22.1$ *sec*, the global diagnosis set is $\mathcal{D}_s^\mathcal{G}(t) = \mathcal{D}_s^\chi \cap \mathcal{D}_s = f_2^{(4)} \cup \{\{\}, f_1^{(3)}, f_2^{(3)}\}$. For $22.1 \leqslant t < 25.3$ *sec* the local decision vectors and diagnosis sets for all the agents remain the same. The new decision vector $D^{(3)}(t) = [1\ 1\ 0]^\top$, does not influence the diagnosis. As D_s^χ also remains unchanged, the resulting global diagnosis set $\mathcal{D}_s^\mathcal{G}$ is the same as the previous one. This is also the case for $t \geqslant 25.3$ *sec* despite the local decision vector of $\mathcal{M}^{(4)}$ changing to $D^{(4)}(t) = [0\ 1\ 1]^\top$.

Based on the simulation results, the proposed diagnosis methodology manages to isolate the actual sensor faults in $S^{(3)}\{1\}$ and $S^{(4)}\{2\}$. Faults were isolated in two out of the four subsystems and in three out of the ten existing sensors in the system. Moreover, the diagnosis sets always included the actual sensor fault(s) in the system.

6. CONCLUSION

In this paper, we illustrated a Distributed SFDI methodology for use in marine fuel engines. The core of the diagnosis approach consists of two layers; one based on a bank of local monitoring agents monitoring specific sensor sets and a global decision logic layer where decisions on the propagation of faults between the different subsystems take place. The goal of the proposed combinatorial decision logic was the isolation of sensor faults affecting multiple sensors of the engine using the information exchanged between its different subsystems. The simulation results showed the efficiency of the proposed method. Future work will include the performance analysis of the designed modules as well as improvements in the design of algebraic residuals and adaptive thresholds using more advanced tools (e.g. SIVIA).

REFERENCES

Aslam, S., Michaelides, M.P., and Herodotou, H. (2020). Internet of Ships: A Survey on Architectures, Emerging Applications, and Challenges. *IEEE Internet of Things Journal*, 7(10), 9714–9727.

Boem, F., Ferrari, R.M., Keliris, C., Parisini, T., and Polycarpou, M.M. (2017). A Distributed Networked Approach for Fault Detection of Large-Scale Systems. *IEEE Transactions on Automatic Control*, 62(1), 18–33.

European Maritime Safety Agency (2020). Annual Overview of Marine Casualties and Incidents 2020. 12–24.

Geertsma, R.D., Negenborn, R.R., Visser, K., Loonstijn, M.A., and Hopman, J.J. (2017). Pitch control for ships with diesel mechanical and hybrid propulsion: Modelling, validation and performance quantification. *Applied Energy*, 206(April), 1609–1631.

Hu, J., Wang, J., Zeng, J., and Zhong, X. (2018). Model-based temperature sensor fault detection and fault-tolerant control of urea-selective catalyst reduction control systems. *Energies*, 11(7).

Jaulin, L. and Walter, E. (1993). Set inversion via interval analysis for nonlinear bounded-error estimation. *Automatica*, 29(4), 1053–1064.

Jones, N.B. and Li, Y.H. (2000). A review of condition monitoring and fault diagnosis for diesel engines. *Tribo Test*, 6(3), 267–291.

Keliris, C., Polycarpou, M.M., and Parisini, T. (2015). Distributed fault diagnosis for process and sensor faults in a class of interconnected input-output nonlinear discrete-time systems. *International Journal of Control*, 88(8), 1472–1489.

MACSEA (2012). Sensors – the Eyes and Ears of Ship Automation. 1–9.

Mesbahi, E. (2001). An intelligent sensor validation and fault diagnostic technique for diesel engines. *Journal of Dynamic Systems, Measurement and Control, Transactions of the ASME*, 123(1), 141–144.

Reppa, V., Polycarpou, M.M., and Panayiotou, C.G. (2016). Sensor fault diagnosis. *Foundations and Trends in Systems and Control*, 3(1-2), 1–248.

Vemuri, A.T., Polycarpou, M.M., and Ciric, A.R. (2001). Fault diagnosis of differential-algebraic systems - Systems, Man and Cyb ernetics, Part A, IEEE Transactions on. 31(2), 143–152.

Wang, Y., Zhang, F., and Cui, T. (2017). Fault diagnosis and fault-tolerant control for Manifold Absolute Pressure Sensor (MAP) of diesel engine based on Elman network observer. *Control Engineering and Applied Informatics*, 19(2), 90–100.

Wohlthan, M., Schadler, D., Pirker, G., and Wimmer, A. (2021). A multi-stage geometric approach for sensor fault isolation on engine test beds. *Measurement: Journal of the International Measurement Confederation*, 168(May 2020), 108313.

Wu, N.E., Thavamani, S., Zhang, Y.M., and Blanke, M. (2006). Sensor fault masking of a ship propulsion system. *Control Engineering Practice*, 14(11), 1337–1345.